



Extraction of lithium from coal fly ash by low-temperature ammonium fluoride activation-assisted leaching

Haiqing Xu^b, Chunli Liu^{a,*}, Xue Mi^a, Zhongbing Wang^a, Junwei Han^{c,*}, Guisheng Zeng^a, Pengfei Liu^a, Qian Guan^a, Haiyan Ji^a, Shuzhen Huang^a

^a Key Laboratory of Jiangxi Province for Persistent Pollutants Control and Resources Recycle, School of Environment and Chemical Engineering, Nanchang Hangkong University, Nanchang 330063, China

^b Beijing Cycle Columbus Environmental Science and Technology Co., Ltd, Beijing 100190, China

^c School of Minerals Processing and Bioengineering, Central South University, Changsha, Hunan 410083, China



ARTICLE INFO

Keywords:

Ammonium fluoride
Activation leaching
Coal fly ash
Lithium

ABSTRACT

A novel process for extracting lithium from coal fly ash by low-temperature salt activation with ammonium fluoride was proposed in this study. The glass phase in coal fly ash was converted to water-soluble fluoride salts after the salt activation process, which was followed by the extraction of lithium from the glass phase via water leaching. The effects of activation temperature and $\text{SiO}_2/\text{NH}_4\text{F}$ mass ratio on the extraction of lithium were investigated in detail. The results showed that more than 90% of lithium was recovered under the optimized conditions: 155 °C of activation temperature, 1:1.35 of $\text{SiO}_2/\text{NH}_4\text{F}$ mass ratio. A possible reaction mechanism for lithium extraction was also proposed based on thermodynamic, thermogravimetry, X-ray diffraction, scanning electron microscopy, and solid nuclear magnetic resonance analyses. This work provides a unique platform reference for further studies on the efficient extraction of resources with similar mineral compositions.

1. Introduction

Lithium is the lightest alkali metal in the world. With the burgeoning development and large-scale application of lithium-ion batteries (LIBs), the demand for lithium has grown tremendously in recent years [1,2]. For example, the global production of lithium increased by 23 % in 2018 according to the U.S. Geological Survey [3]. Currently, China is the leading country in developing LIBs and the world's largest consumer of lithium, accounting for 50 % of the global consumption [4]. It is predicted that the proven reserves of lithium resources in China can meet the demand for LIBs production only until the year 2028 [5]. Given the increasingly tense supply–demand situation and the criticality of lithium resources, sustainable and practical ways to recover lithium from new unconventional alternative sources are urgently needed [6–9].

Coal is the primary fossil energy resource used for power generation in China [10]. Large quantities of coal that are rich in aluminum and lithium have been found in many coalfields located in the central–western regions of Inner Mongolia and the northern Shanxi Province, China [11–13]. These metals can be enriched in coal fly ash (CFA) by coal combustion. The content of Li_2O in CFA is approximately

0.06–0.30 wt% [14,15]; this is comparable to industrial grade Li-bearing pegmatite deposits in China, which have Li_2O contents of 0.2 wt% (DZ/T 0203–2002, 2003). Thus, CFA containing Li_2O is advantageous as a lithium resource.

To support the development of lithium recovery technology from CFA, several studies have investigated the distribution and modes of occurrence of lithium in different CFA obtained from Shanxi Province and Inner Mongolia, China [16,17]. Currently, vast majority of coal ash produced by coal-fired power plants is pulverized coal furnace-type CFA, comprising mullite/corundum crystalline phases and a silica-rich aluminosilicate glass phase with which lithium is primarily associated [18,19]. Thus, to effectively extract lithium from CFA, it is necessary to separate the aluminosilicate glass phase to liberate lithium. Acid–alkali combination and the biological leaching are two of the main methods to recovery lithium from CFA. Hu et al. [19] studied the distribution of lithium in CFA and its recovery via an acid–alkali combination process. They found that 79–94 % of the lithium was present in the glass phase, with the remaining 5–16 % in the crystalline phases. Ma et al. [20] found that 80 % of lithium and 72 % of gallium in CFA could be extracted using a moderate acid–alkali-based alternate method. However, this process

* Corresponding authors.

E-mail addresses: clius19@126.com (C. Liu), hanjunwei2008@163.com (J. Han).

requires not only large amounts of chemicals, but also complex operations and numerous steps. The biological leaching process has also attracted significant attentions due to its mild leaching conditions and high operating safety [21,22]. The bottleneck of this process is the difficult strain culture and the long leaching time, which severely curtails its industrial adoption [23].

In this study, a low-temperature ammonium fluoride activation-assisted water leaching process was adopted to recover lithium from CFA. Ammonium fluoride in the activation process can destroy the Si-O-Al coordination structure of the aluminosilicate in the glass phase and obtain high reactivity and water-soluble products, based on the difference in the reaction difficulty between the glass phase and crystalline phase in CFA with ammonium fluoride [24,25]. And then, lithium can be extracted by water leaching after activation. The effects of the ammonium fluoride activation conditions, including the SiO₂/NH₄F mass ratio and activation temperature, on the extraction efficiency of lithium were also studied in detail. The mechanism of low-temperature ammonium fluoride activation was systematically analyzed.

2. Materials and methods

2.1. Materials

CFA was provided by a pulverized coal furnace of a thermoelectric power plant in Inner Mongolia Autonomous Region, China. Analytical grade ammonium fluoride (Sinopharm Group, greater than 99 wt%) was used as an activator. All solutions were produced or diluted using deionized water.

2.2. Experimental process

A schematic of the experimental process is shown in Fig. 1. The key to the entire process is ammonium fluoride activation and water leaching. The first step was to transform the glass phase into a water-soluble product; the second step involved dissolving the water-soluble product and extracting lithium.

Ammonium fluoride activation was performed in a tubular furnace. A mixture of CFA and ammonium fluoride at various SiO₂/NH₄F mass ratios was placed in covered alumina crucibles, heated to 125–160 °C for 120 min, and then cooled to ambient temperature. After activation, the activated samples were leached using distilled water at 70 °C with a liquid-solid ratio of 10 ml/g for 120 min. The leaching slurry was filtered to obtain the leaching residue and lixivium. The leaching

efficiency of lithium was calculated by Eq. (1).

$$\frac{cV}{m_0} \quad (1)$$

where η is leaching efficiency of lithium, V is the volume of lixivium, c is the concentration of lithium in the lixivium, and m_0 is the mass of lithium in CFA before activation. Three parallel experiments were repeated to ensure the repeatability of the results.

2.3. Characterization methods

X-ray fluorescence spectrometer (AXIOS-MAX, 50 kV, 60 mA, integration time of 40 s) was used to examine the chemical composition of the major elements in solid samples. The CFA sample was dissolved in an acid medium (40 wt% HF: 30 wt% H₂O₂: 65 wt% HNO₃ = 1:2:5, v/v) to determine the lithium content by inductively coupled plasma mass spectrometry (ICP-MS, iCAP RQ, Thermo Fisher Scientific, USA) [19,26]. Morphological analyses were conducted using scanning electron microscopy (SEM, JSM-6701F, JEOL Ltd.). The phases of the samples were determined by X-ray diffraction (XRD, X'Pert Pro MPD, Malvern Panalytical; 40 kV, 30 mA, $2\theta = 5\text{--}90^\circ$) with Cu-K α radiation at a scan rate of 0.05°·s⁻¹. The thermochemical behavior was examined using a thermogravimetric analyzer (TG, Mettler Toledo, Switzerland) at a heating rate of 5 °C·min⁻¹ from 30 to 500 °C in an air atmosphere. The solid-state ²⁹Si MAS-NMR spectra of the samples were obtained using a Bruker Corporation AVANCEIII instrument with a 4 mm probe at a spinning frequency of 8.0 kHz. Deconvolution of the ²⁹Si MAS spectra was conducted using Origin2018.

3. Results and discussion

3.1. Characterization of CFA

As shown in Table 1, the content of Al₂O₃ in CFA is 49.56 wt%; the content of Li is 403 µg/g, which is higher than that in CFA. The XRD patterns of the CFA are presented in Fig. 2a. The major crystalline phases in CFA are mullite and corundum; further, the sample has a broad diffraction peak at $2\theta = 19\text{--}25^\circ$, which indicates that the glass phase is amorphous [25]. Fig. 2b indicates that the CFA is mainly consisted of spheroidal particles and has a smooth surface; however, there are some irregular particles, and some smaller particles, which are attached to the surface of larger particles.

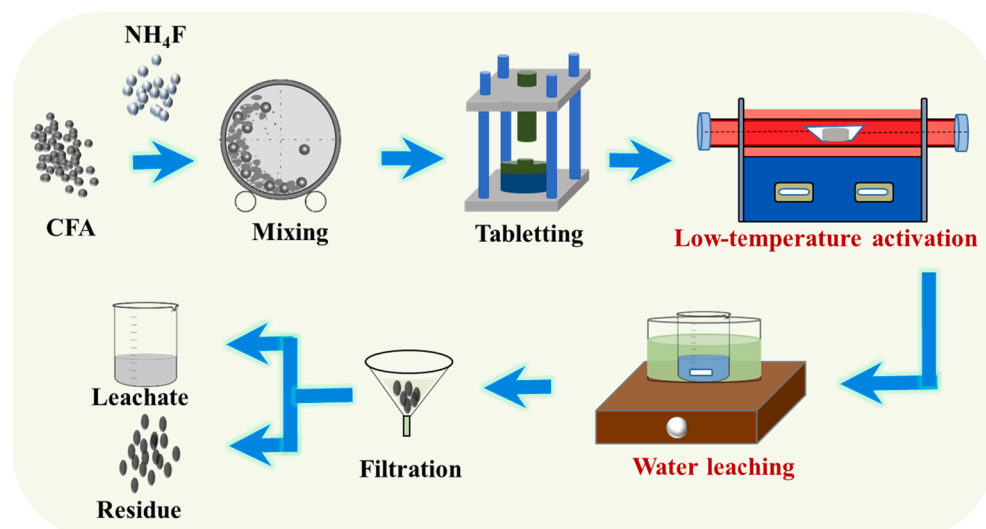


Fig. 1. Flow diagram of lithium recycling from CFA.

Table 1

Major composition and Li concentration in CFA.

Composition	Al ₂ O ₃	SiO ₂	Fe ₂ O ₃	TiO ₂	CaO	MgO	Li	LOI
Contents	49.56	38.72	2.06	1.45	2.35	0.26	403	2.75

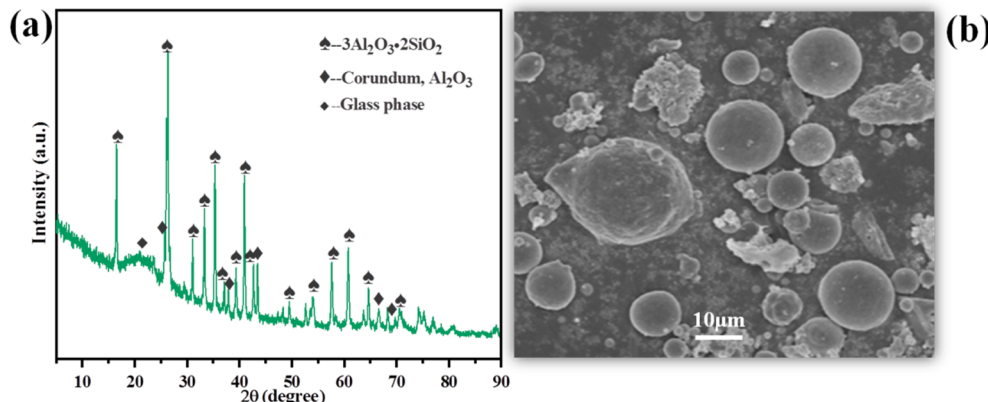
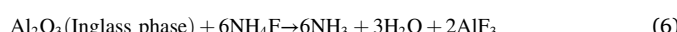
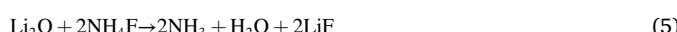
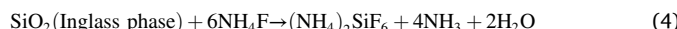
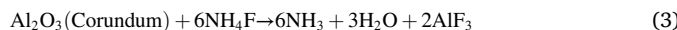
Contents of the major composition and Li are reported in wt% and $\mu\text{g/g}$, respectively. Loss on ignition (LOI) is reported in wt%.

Fig. 2. XRD analysis (a) and SEM images (b) of raw CFA.

3.2. Thermodynamic analysis of the activation process

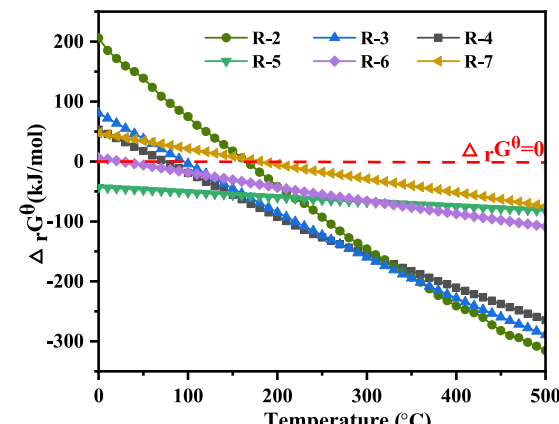
The thermodynamic analysis of the activation process of the glass phase with ammonium fluoride was performed by varying the temperature from 0 to 500 °C. Apart from amorphous silica and alumina, the vast majority of impurities are mainly contained in the glass phase [16]. Which may due to the rapidly quench of CFA as it exited the combustion zone during the coal combustion process, leaving no time for amorphous silica and the other oxidation phases to form a crystalline state and generate an amorphous glass matrix. According to the mineralogical characteristics, the possible reactions are as follows:



The Gibbs free energies $\Delta_f G^\ominus$ of the reactions (R-2–R-7) at different temperatures are shown in Fig. 3. Compared to reactions (R-2), (R-3), and (R-7), the Gibbs free energy of reactions (R-4, R-5, R-6) is negative at lower temperatures, suggesting that the mineral compositions in the glass phase can react with ammonium fluoride at different temperatures. Furthermore, the reactions in which the crystalline phases react with ammonium fluoride are less thermodynamically favorable than those in the glass phase and require more stringent conditions.

3.3. Extracting lithium through ammonium fluoride activation

The relationship between the mass ratio of SiO₂/NH₄F and the leaching efficiency of lithium is shown in Fig. 4a. The leaching efficiency of lithium increases gradually from 32.56 % to 90.82 % when the mass ratio of SiO₂/NH₄F increases from 1:0.75 to 1:1.35, indicating that the amount of ammonium fluoride has a crucial influence on it. With a further increase in the mass ratio, the leaching efficiency remains constant. The XRD results (Fig. 4c) show that a new (NH₄)₂SiF₆ phase

Fig. 3. Relationship between $\Delta_f G^\ominus$ and temperature for reactions (calculated by HSC 6.0).

appears in the activated product when the mass ratio of SiO₂/NH₄F is 1:0.75. When the amount of ammonium fluoride increases to 1:1.35, the diffraction peaks of (NH₄)₂SiF₆ are dramatically strengthened, whereas, those of the mullite ($3\text{Al}_2\text{O}_3 \cdot 2\text{SiO}_2$) and corundum ($\alpha\text{-Al}_2\text{O}_3$) remain unchanged, demonstrating that ammonium fluoride reacted only with the glass phase. Meanwhile, the active products have the same diffraction peaks when the mass ratios of SiO₂/NH₄F are 1:1.35 and 1:1.5, indicating that the glass phase decomposition reaction was fully completed at a mass ratio of 1:1.35. The peaks of (NH₄)₃AlF₆ and Ca₃Al₂O₆(H₂O)₆ can be observed in the spectrum, which is attributed to the reaction of ammonium fluoride with CaO and amorphous alumina derived from the glass phase. The pH of the subsequent water leaching solution was approximately 4.5. Therefore, (NH₄)₃AlF₆, Ca₃Al₂O₆(H₂O)₆, lithium compounds, and other fluoride salts in the activated product could be decomposed during the water leaching process.

Fig. 4b shows the relationship between the activation temperature and the leaching efficiency of lithium while maintaining a mass ratio of SiO₂/NH₄F at 1:1.35. Evidently, the leaching efficiency increased considerably as the activation temperature increased from 125 to 155 °C. The effects of the activation temperature on the phase

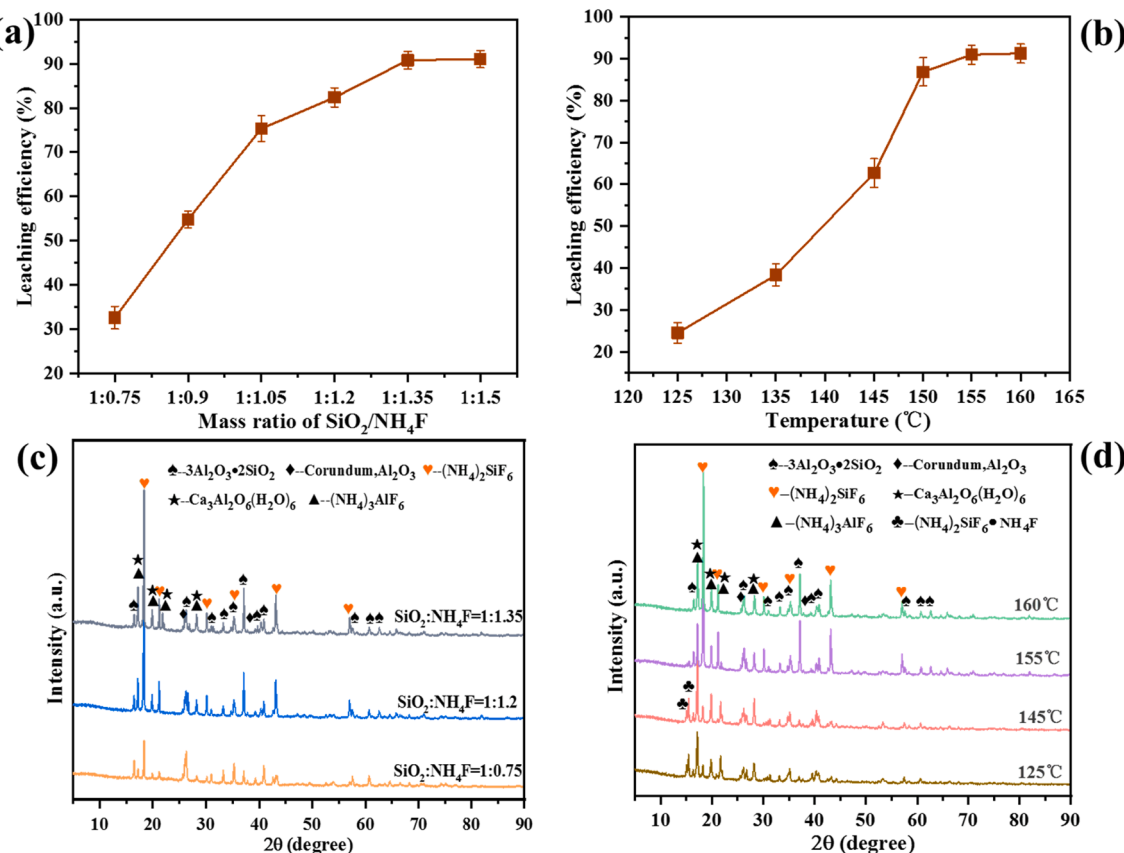


Fig. 4. Leaching efficiency of lithium for different (a) mass ratios of $\text{SiO}_2/\text{NH}_4\text{F}$ and (b) activation temperatures; XRD patterns of the activated products for different (c) mass ratios of $\text{SiO}_2/\text{NH}_4\text{F}$ and (d) activation temperatures.

transformation of the activated products were also studied (Fig. 4d). Diffraction peaks of $(\text{NH}_4)_2\text{SiF}_6$ were detected at 125 $^{\circ}\text{C}$, implying that some of the amorphous silica in the glass phase began to react with ammonium fluoride at this temperature. The $(\text{NH}_4)_2\text{SiF}_6$ phase increased gradually with the increasing of temperatures, whereas no considerable variation was observed for those of mullite ($3\text{Al}_2\text{O}_3 \bullet 2\text{SiO}_2$) and corundum ($\alpha\text{-Al}_2\text{O}_3$), indicating that they did not react with ammonium fluoride in this temperature range, which is consistent with the thermodynamic analysis results.

3.4. Mechanism of extracting lithium

The thermochemical behavior of the mass ratio of $\text{SiO}_2/\text{NH}_4\text{F}$ at

1:1.35 mixing powder is shown in Fig. 5a and can be divided into two significant weight losses. The first significant weight loss occurred under the temperatures range from 90 to 165 $^{\circ}\text{C}$, and that was approximately 12.9 %. As the temperature increased above 90 $^{\circ}\text{C}$, the NH_4F (s) present in the mixture started melting and then decomposed partly to form gaseous substances; it simultaneously reacted with the glass phase to form water-soluble products. This is indicated by the rapid increase in weight loss, which reached a maximum at approximately 126.5 $^{\circ}\text{C}$ [27]. The glass phase gradually decomposed with the increase of temperature, and water-soluble fluoride salt formation reactions were completed at around 165 $^{\circ}\text{C}$. The secondary significant weight loss occurred in the temperatures range from 165 to 356 $^{\circ}\text{C}$, and that was approximately 29.5 %, which could be attributed to the reaction of ammonium fluoride

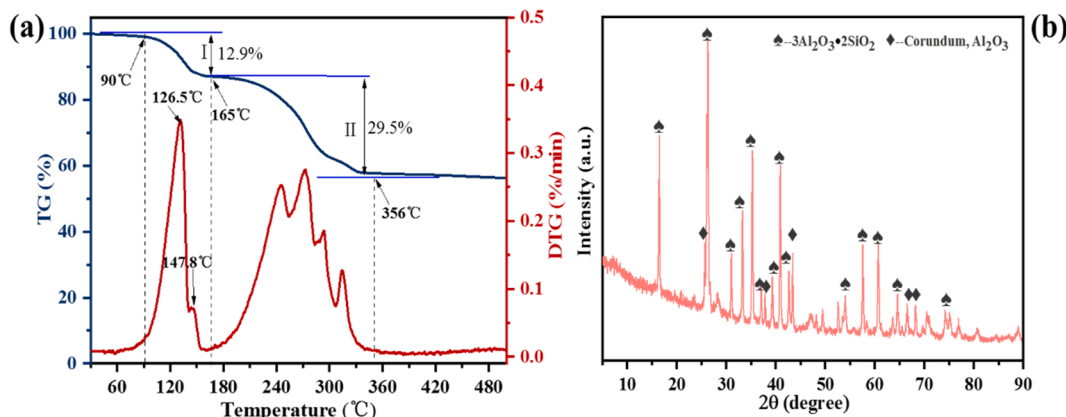


Fig. 5. (a) TG-DTG curve of the 1:1.35 (the mass ratio of $\text{SiO}_2/\text{NH}_4\text{F} = 1:1.35$) mixing powder, (b) XRD pattern of the leached residue.

with the major crystalline phases (mullite and corundum) in CFA. From the data present in the TG-DTG curve, it was determined that the effective activation temperature range for the glass phase in CFA should be between 90 and 165 °C. In addition, XRD (Fig. 5b) results showed that the broad diffraction peak at $2\theta = 19\text{--}25^\circ$ disappeared and only the mullite and corundum phases were observed in the leached residue, indicating that the activation temperature range in Fig. 5a is supported by the XRD patterns.

Fig. 6 shows the ^{29}Si MAS-NMR spectra of the raw CFA and leached residue. As displayed in Fig. 6a, the spectra of the raw CFA exhibit broad resonance in the chemical shift ranging from –80 ppm to –130 ppm. The poorly defined area in the spectra indicates the heterogeneous presence of various silicon sites in the specimen. The resonance peak detected at –115 ppm ($\text{Q}_4(0\text{Al})$) can be attributed to the amorphous silica with $\text{Si}-\text{O}-\text{Si}$ structure, whereas the peak at –92 ppm corresponds to stable crystal mullite [28,29]. The resonance peaks at –84, –95, –100, and –106 ppm are identified as silicon tetrahedrons surrounded by $\text{Q}_2(1\text{Al})$, $\text{Q}_3(1\text{Al})$, $\text{Q}_4(2\text{Al})$, and $\text{Q}_4(3\text{Al})$, respectively, corroborating the presence of polymeric $\text{Si}-\text{O}-\text{Al}$ bonds in glass phase contained in CFA. During ammonium fluoride activation, the $\text{Si}-\text{O}-\text{Si}$, $\text{Si}-\text{O}-\text{Al}$, and other unstable bonds in the glass phase are broken by the powerful chemical force of ammonium fluoride, and the reactivity of the activated sample is improved. The results in Fig. 6b show that most of the amorphous glass phase is dissolved after water leaching treatment. The resonance peaks ascribed to vitreous phases (–84, –106, and –115 ppm) are decreased, and the peak of stable mullite (–92 ppm) is improved (the percentage of area increases from 16.32 % to 61.43 %). Thus, the vast majority of lithium is extracted during the ammonium fluoride activation–water leaching process, wherein the glass phase is thoroughly dissolved.

The morphology of the activated product and leached residue were examined by SEM, as shown in Fig. 7. During ammonium fluoride activation, owing to the decomposition and transformation of the glass phase, the spherical structure of the raw CFA (Fig. 2b) was destroyed; some of the activated products stuck together with a wide range of sizes and rough surfaces (Fig. 7a, b). From the aforementioned results, the products are composed of a glass-phase converter and unreacted crystalline phases. After the water leaching treatment, as seen from Fig. 7c and d, the particle size of the solid sample decreased, and the leached residues were mainly less than 10 μm . The inner structure of the particles was exposed, featuring several interlocking needle-like mullite crystals and some micropores. Similar morphological observations were previously reported by Zhang et al. [30]. Which indicate that ammonium fluoride activation destroy the basic structure of CFA; the glass phase was completely decomposed and transformed. Thus, lithium

encapsulated in the glass phase was extracted effectively via water leaching.

Previous studies have suggested that lithium is primarily present in the glass phase and a small part is presented in CFA [18]. Therefore, to efficiently extract lithium from CFA, the glass phase must be broken completely. Referring to the aforementioned analysis, the possible reaction pathway of CFA ammonium fluoride activation is shown in Fig. 8; it can be described in two reaction steps.

The $\text{Si}-\text{O}$ bonds in the glass phase were destroyed by F^- and water-soluble fluoride salt products were generated on the surface of the CFA particles after the CFA particles interacted with ammonium fluoride. Liquid phases were gradually formed with the generation of a water-soluble product due to the low melting point. Subsequently, the liquid outer layer became a barrier between the F^- ions and the unreacted inner core. Meanwhile, a few F^- diffused into the reaction interface. Therefore, by further increasing the temperature, the amount of the liquid phase gradually increased, and the unreacted particles were gradually wrapped by fluoride salt melt.

The NH_4F extended the melting point when it increased to the holding temperature. The liquid phase contained a large amount of F^- ions that destroyed the barrier between the unreacted inner core and the fluoride salt melt. The $\text{Si}-\text{O}$ - bonds in the glass phase are disrupted during a short period. During the holding process, the amorphous silica and lithium in the glass phase were gradually converted into water-soluble fluoride salts.

Finally, lithium can be recycled by water leaching at a mild temperature, whereas the crystalline phases (mullite and corundum) in CFA are separated as filter residues.

4. Conclusions

A novel method, including ammonium fluoride activation and water leaching, was developed to extract lithium from coal fly ash. Lithium was released from the glass phase in CFA by using ammonium fluoride activation. More than 90 % of lithium was extracted at 155 °C and $\text{SiO}_2/\text{NH}_4\text{F}$ mass ratio of 1:1.35. The lithium recovery process was also studied via thermodynamic calculations, thermogravimetry, XRD, ^{29}Si MAS-NMR characterization, and SEM observations. The results demonstrated that the reaction of the glass phase with NH_4F was thermodynamically more favorable than that of mullite and corundum. During ammonium fluoride activation, $\text{Si}-\text{O}$ - bonds were effectively broken in the glass phase, and the amorphous silica and lithium were converted into water-soluble fluoride salts. Then, lithium was leached by water leaching, whereas the crystalline phases (mullite and corundum) in CFA are separated as residues. In conclusion, this study provides a promising

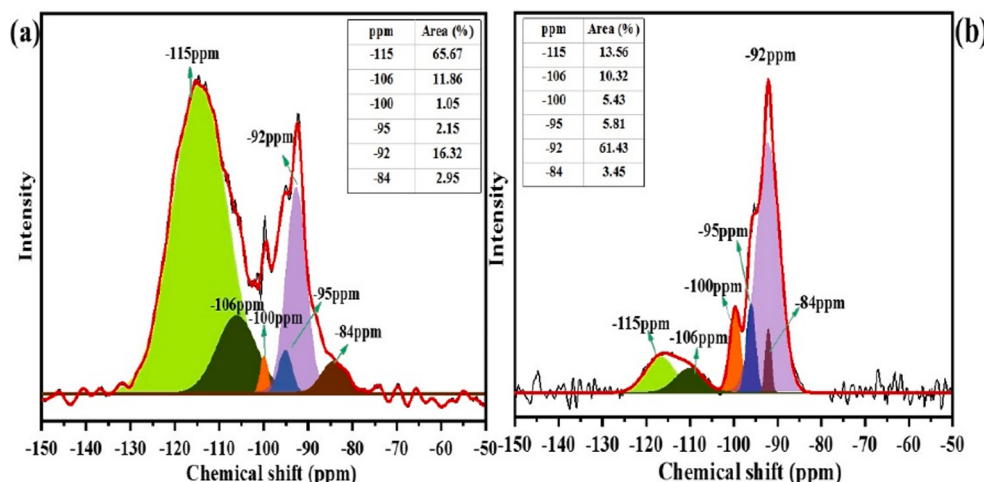


Fig. 6. ^{29}Si MAS-NMR spectra of (a) raw CFA and (b) leached residue.

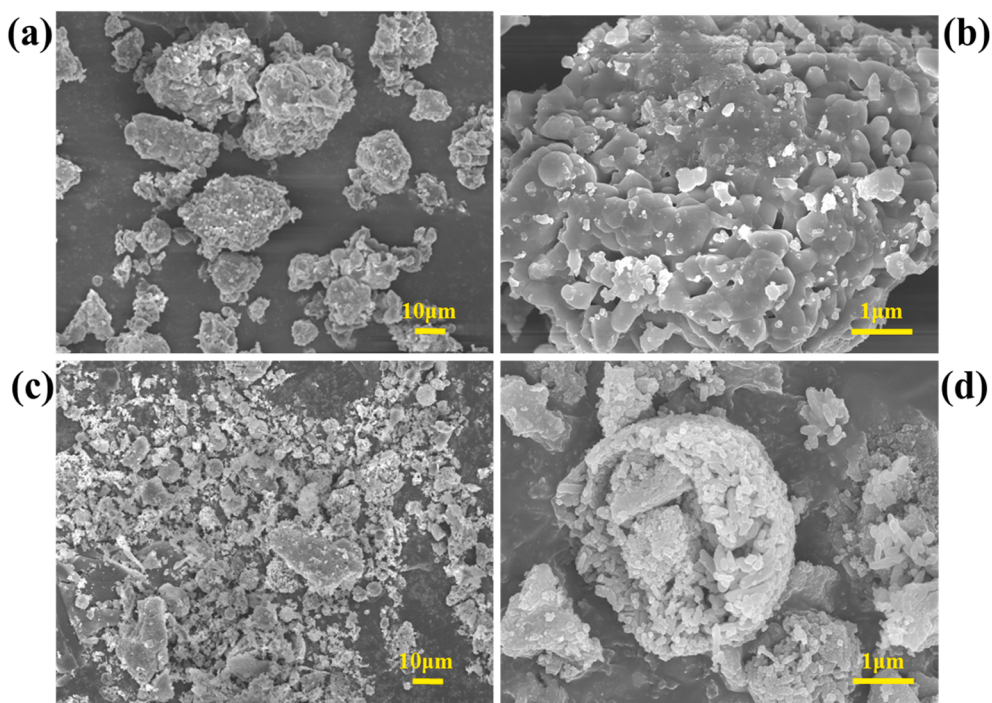


Fig. 7. SEM images of (a), (b) activated product and (c), (d) leached residue.

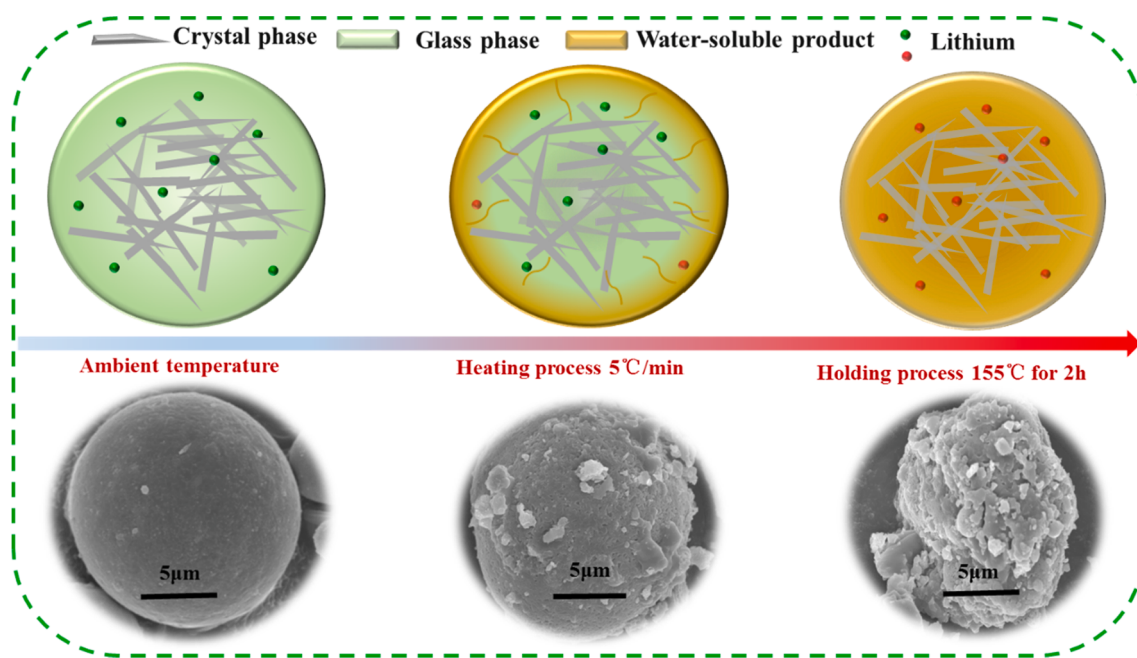


Fig. 8. Possible reaction pathway of CFA ammonium fluoride activation.

technology for lithium recovery from CFA.

CRediT authorship contribution statement

Haiqing Xu: Writing-original draft, Investigation, Methodology, Visualization. **Chunli Liu:** Writing-review & editing, Conceptualization, Formal analysis, Supervision, Funding acquisition. **Xue Mi:** Conceptualization, Supervision, Data curation. **Zhongbing Wang:** Investigation, Formal analysis, Software. **Junwei Han:** Writing-review & editing, Investigation, Methodology, Funding acquisition. **Guisheng Zeng:** Conceptualization, Validation. **Pengfei Liu:** Data curation,

Validation. **Qian Guan:** Data curation, Software. **Haiyan Ji:** Supervision, Visualization. **Shuzhen Huang:** Validation, Supervision.

Declaration of Competing Interest

The authors declare that they have no known competing financial interests or personal relationships that could have appeared to influence the work reported in this paper.

Acknowledgements

This study was financially supported by the National Key Research and Development Program of China (No. 2019YFC1907900), the Key Project of Research and Development Plan of Jiangxi Province (No. 20201BBE51007), Natural Science Foundation of Hunan Province (No. 2021JJ20062), and Innovation Driven Project of Central South University (No. 2020CX038).

References

- [1] W. Zhang, A. Noble, X. Yang, R. Honaker, Lithium leaching recovery and mechanisms from density fractions of an Illinois Basin bituminous coal, *Fuel* 268 (2020) 117319, <https://doi.org/10.1016/j.fuel.2020.117319>.
- [2] F. Wu, J. Maier, Y. Yu, Guidelines and trends for next-generation rechargeable lithium and lithium-ion batteries, *Chem. Soc. Rev.* 49 (5) (2020) 1569–1614, <https://doi.org/10.1039/C7CS00863E>.
- [3] Survey USG. Mineral Commodity Summaries, 2009. Government Printing Office; 2019.
- [4] J. Song, W. Yan, H. Cao, Q. Song, H. Ding, Z. Lv, Y. Zhang, Z. Sun, Material flow analysis on critical raw materials of lithium-ion batteries in China, *J. Clean. Prod.* 215 (2019) 570–581, <https://doi.org/10.1016/j.jclepro.2019.01.081>.
- [5] D. Qiao, G. Wang, T. Gao, B. Wen, T. Dai, Potential impact of the end-of-life batteries recycling of electric vehicles on lithium demand in China: 2010–2050, *Sci. Total Environ.* 764 (2021) 142835, <https://doi.org/10.1016/j.scitotenv.2020.142835>.
- [6] H. Gu, T. Guo, H. Wen, C. Luo, Y.i. Cui, S. Du, N. Wang, Leaching efficiency of sulfuric acid on selective lithium leachability from bauxitic claystone, *Miner. Eng.* 145 (2020) 106076, <https://doi.org/10.1016/j.mineng.2019.106076>.
- [7] Y. Zhang, J. Zhang, L. Wu, L. Tan, F. Xie, J. Cheng, Extraction of lithium and aluminium from bauxite mine tailings by mixed acid treatment without roasting, *J. Hazard. Mater.* 404 (2021) 124044, <https://doi.org/10.1016/j.jhazmat.2020.124044>.
- [8] H. Dang, N.a. Li, Z. Chang, B. Wang, Y. Zhan, X. Wu, W. Liu, S. Ali, H. Li, J. Guo, W. Li, H. Zhou, C. Sun, Lithium leaching via calcium chloride roasting from simulated pyrometallurgical slag of spent lithium ion battery, *Sep. Purif. Technol.* 233 (2020) 116025, <https://doi.org/10.1016/j.seppur.2019.116025>.
- [9] C. Liu, J. Lin, H. Cao, Y. Zhang, Z. Sun, Recycling of spent lithium-ion batteries in view of lithium recovery: A critical review, *J. Clean. Prod.* 228 (2019) 801–813, <https://doi.org/10.1016/j.jclepro.2019.04.304>.
- [10] M. Wang, R. Dewil, K. Maniatis, J. Wheeldon, T. Tan, J. Baeyens, Y. Fang, Biomass-derived aviation fuels: Challenges and perspective, *Prog. Energy Combust. Sci.* 74 (2019) 31–49, <https://doi.org/10.1016/j.pecs.2019.04.004>.
- [11] S. Dai, R. Finkelman, Coal as a promising source of critical elements: Progress and future prospects, *Int. J. Coal Geol.* 186 (2018) 155–164, <https://doi.org/10.1016/j.coal.2017.06.005>.
- [12] Y. Sun, C. Zhao, J. Zhang, J. Yang, Y. Zhang, Y. Yuan, J. Xu, D. Duan, Concentrations of valuable elements of the coals from the Pingshuo mining district, ningwu coalfield, northern China, *Energy Explor. Exploit.* 31 (5) (2013) 727–744, <https://doi.org/10.1260/0144-5987.31.5.727>.
- [13] B. Liu, J. Wang, H. He, V. Mishra, Y. Li, J. Wang, C. Zhao, Geochemistry of Carboniferous coals from the Laoyaogou mine, Ningwu coalfield, Shanxi Province, northern China: Emphasis on the enrichment of valuable elements, *Fuel* 279 (2020) 118414, <https://doi.org/10.1016/j.fuel.2020.118414>.
- [14] B. Gong, C. Tian, Z. Xiong, Y. Zhao, J. Zhang, Mineral changes and trace element releases during extraction of alumina from high aluminum fly ash in Inner Mongolia, China. *Int. J. Coal Geol.* 166 (2016) 96–107, <https://doi.org/10.1016/j.coal.2016.07.001>.
- [15] S. Dai, X. Yan, C.R. Ward, J.C. Hower, L. Zhao, X. Wang, L. Zhao, D. Ren, R. Finkelman, Valuable elements in Chinese coals: A review, *International Geology Review.* 60 (5–6) (2018) 590–620.
- [16] S. Dai, L. Zhao, S. Peng, C.-L. Chou, X. Wang, Y. Zhang, D. Li, Y. Sun, Abundances and distribution of minerals and elements in high-alumina coal fly ash from the Jungar power plant, Inner Mongolia, China. *Int. J. Coal Geol.* 81 (4) (2010) 320–332, <https://doi.org/10.1016/j.coal.2009.03.005>.
- [17] S. Dai, L. Zhao, J.C. Hower, M.N. Johnston, W. Song, P. Wang, S. Zhang, Petrology, mineralogy, and chemistry of size-fractionated fly ash from the Jungar power plant, Inner Mongolia, China, with emphasis on the distribution of rare earth elements, *Energy Fuel* 28 (2) (2014) 1502–1514, <https://doi.org/10.1021/ef402184t>.
- [18] J. Ding, S. Ma, S. Shen, Z. Xie, S. Zheng, Y. Zhang, Research and industrialization progress of recovering alumina from fly ash: A concise review, *Waste Management* 60 (2017) 375–387, <https://doi.org/10.1016/j.wasman.2016.06.009>.
- [19] P. Hu, X. Hou, J. Zhang, S. Li, H. Wu, A. Damø, H. Li, Q. Wu, X. Xi, Distribution and occurrence of lithium in high-alumina-coal fly ash, *Int. J. Coal Geol.* 189 (2018) 27–34, <https://doi.org/10.1016/j.coal.2018.02.011>.
- [20] Z. Ma, S. Zhang, H. Zhang, F. Cheng, Novel extraction of valuable metals from circulating fluidized bed derived high-alumina fly ash by acid-alkaline based alternate method, *J. Clean. Prod.* 230 (2019) 302–313, <https://doi.org/10.1016/j.jclepro.2019.05.113>.
- [21] HaiFeng Su, F. Tan, JiaFu Lin, An integrated approach combines hydrothermal chemical and biological treatment to enhance recycle of rare metals from coal fly ash, *Chem. Eng. J.* 395 (2020) 124640, <https://doi.org/10.1016/j.cej.2020.124640>.
- [22] HaiFeng Su, H. Chen, JiaFu Lin, A sequential integration approach using Aspergillus Niger to intensify coal fly ash as a rare metal pool, *Fuel* 270 (2020) 117460, <https://doi.org/10.1016/j.fuel.2020.117460>.
- [23] X. Fan, S. Lv, J. Xia, Z. Nie, D. Zhang, X. Pan, L. Liu, W. Wen, L. Zheng, Y. Zhao, Extraction of Al and Ce from coal fly ash by biogenic Fe³⁺ and H₂SO₄, *Chem. Eng. J.* 370 (2019) 1407–1424, <https://doi.org/10.1016/j.cej.2019.04.014>.
- [24] S.M. Sharafeev, V.M. Pogrebennikov, Phase Formation Processes in Natural Magnesium Silicates of Various Structures by Ammonium Fluoride Treatment, *Refract. Ind. Ceram.* 61 (2) (2020) 200–206, <https://doi.org/10.1007/s11148-020-00456-6>.
- [25] G. Han, S. Yang, W. Peng, Y. Huang, H. Wu, W. Chai, J. Liu, Enhanced recycling and utilization of mullite from coal fly ash with a flotation and metallurgy process, *J. Clean. Prod.* 178 (2018) 804–813, <https://doi.org/10.1016/j.jclepro.2018.01.073>.
- [26] F. Low, L. Zhang, Microwave digestion for the quantification of inorganic elements in coal and coal ash using ICP-OES, *Talanta* 101 (2012) 346–352, <https://doi.org/10.1016/j.talanta.2012.09.037>.
- [27] A.N. D'yachenko, R.I. Kraidenko, Fluorination of germanium concentrates with ammonium fluorides, *Russ J Appl Chem* 81 (6) (2008) 952–955, <https://doi.org/10.1134/S1070427208060050>.
- [28] X. Gao, Q.L. Yu, H.J.H. Brouwers, Apply ²⁹Si, 27Al MAS NMR and selective dissolution in identifying the reaction degree of alkali activated slag-fly ash composites, *Ceram. Int.* 43 (15) (2017) 12408–12419, <https://doi.org/10.1016/j.ceramint.2017.06.108>.
- [29] C. Yang, J. Zhang, S. Li, H. Li, X. Hou, G. Zhu, Mechanisms of mechanochemical activation during comprehensive utilization of high-alumina coal fly ash, *Waste Management* 116 (2020) 190–195, <https://doi.org/10.1016/j.wasman.2020.08.003>.
- [30] J. Zhang, S. Li, H. Li, M. He, Acid activation for pre-desilication high-alumina fly ash, *Fuel Process. Technol.* 151 (2016) 64–71, <https://doi.org/10.1016/j.fuproc.2016.05.036>.